Supporting Information

In-situ fabrication and designing of a novel electrochemical sensor based on $Ag_{3.84}Sn_3S_8$@rGO nanocomposite for a competitive ultra-detection of metronidazole in human urine

Jit Satra[a], Papri Mondal[a], Gopala Ram Bhadu[b] and Bibhutosh Adhikary[*a]

[*] Corresponding authors

[a] Department of Chemistry, Indian Institute of Engineering Science and Technology, Shibpur, Howrah 711 103, West Bengal, India

Email: bibutoshadhikary@gmail.com

[b] Department of Analytical and Environmental Science Division and Centralized Instrument Facility, Gijubhai Badheka Marg, Bhavnagar 364021, Gujarat, India

Chemicals and materials

H_3PO_4 (≥ 85%), $KMNO_4$, HCl (37%) were purchased from Spectrochem. Pvt. Ltd. (India). Graphite powder (<20 mM), H_2SO_4 (99.99%), L-Ascorbic acid (99%), $AgNO_3$ (98%), $SnCl_2 \cdot 2H_2O$ (99.99%), CH_4N_2S (99%), EtOH (99.99%), nafion (5 wt%), α-Al_2O_3, 0.45μm PVDF hydrophilic membrane, MNZ, ODZ, OXN, CFX, TDE, IZE, 5-NIZ, 4-NP, 4-NB, Hg and UA were purchased from Sigma-Aldrich (India). All experiments were performed in DI water.

Physical Measurement

Powder X-ray diffraction studies have been done using a PAN analytical X-ray diffractometer having monochromatic CuKα radiation (λ = 1.540598 Å). Infrared spectra were obtained in the range of 4000–400 cm−1 by JASCO FT-IR-460 Plus. To evaluate the elemental composition, Energy dispersed X-ray (EDX) analysis was performed using a JEOL JSM-7100F. Shape and morphologies were studied using a radiation source JEOL JEM-2100 transmission electron microscope (TEM) working at 200 kV. X-ray photoelectron spectroscopy (XPS) was performed by Perkin-Elmer Physical Electronics 5600 spectrometer. Diffuse reflectance spectroscopy (DRS) was undergone by Agilent Cary 5000. The surface area of the samples has been obtained by an automatic gas adsorption/desorption analyzer (Quantachrome Instruments, version 3.01) with N_2 as adsorbate. The corresponding samples were degassed in vacuum at 220 °C for 24 h before test. The specific surface areas of the samples were calculated by the Brunauer-Emmett-Teller (BET) method using the adsorption S-3 branch in $P_{relative}$ range from 0.05-0.30.

Fabrication of ITO coated glass slides with catalysts for chronoampermetric measurement

The modification was done by the following procedures; (1) the ITO coated glass slides are thoroughly cleaned in soap water followed by acetone and iso-propanol by ultrasonication for 12

hours and dried in hot air oven at 100 ^{0}C, (2) the catalyst was dispersed in toluene and ultrasonicated for 1 hour, (3) then the fabrication was done by spin-coating method in which each time 100 µL of as prepared dispersed solution was dropped onto the surface of the glass slide and spin-coated by 10000 RPM and lastly (4) the fabricated glass slides were dried over hot plate at 120 ^{0}C.

Photocatalytic activity measurement

The whole photocatalytic reaction was performed in a 50 ml beaker and the MNZ concentration was maintained at 30 mg/L (recorded on a JASCO V-530 UV-Vis spectrophotometer). The catalyst concentration was optimized to 20 mg/ml by varying five different set of concentration and the illuminating white light power density was maintained at 1 sun (100 $mW \cdot cm^{-2}$) which is equipped with 420 nm cut-off filter (Newport-Oriel Instruments, USA) to access only visible light. After each photocatalytic cycle the main mixture was filtered by 0.45 µm PVDF membranes and the absorption spectra were studied. The reusability of the photocatalyst was evaluated only after recollecting the catalyst followed by washing through centrifugation repeatedly and then drying at the end of each cycle.

Fabrication of working electrode and electrochemical experiments

Before modification, the conducting surface of the glassy carbon electrode (GCE) (here the working electrode) was vertically immersed and thoroughly cleaned by ultrasonication in acetone then isopropanol followed by DI water for a whole day. Then the electrode surface was polished with α-Al_2O_3 (with different size) slurry in DI water and dried overnight in a closed glass vessel. Next for the conducting layer of the sensor a suspension was made by mixing 0.5% of nafion of 1 ml and NC in DI water. To homogenize, it was ultrasonicated for 2 hr. Then 10 µL of the suspension was drop casted onto the cleaned and polished electrode surface. It was then

allowed to dry in hot air oven for 30 mins and the electrodes were rinsed in DI water slowly to remove lightly attached NC particles. It is to be noted that the surface area of the working electrode was maintained at 0.126 cm^2. The characteristic electrochemical parameters like concentration of analyte, scan rate and pH value were optimized by CV in PBS electrolyte. The whole electrochemical experiments were undergone by CHI 7014E workstation through three electrode system where reference electrode and counter electrode are Ag/AgCl and Pt wire.

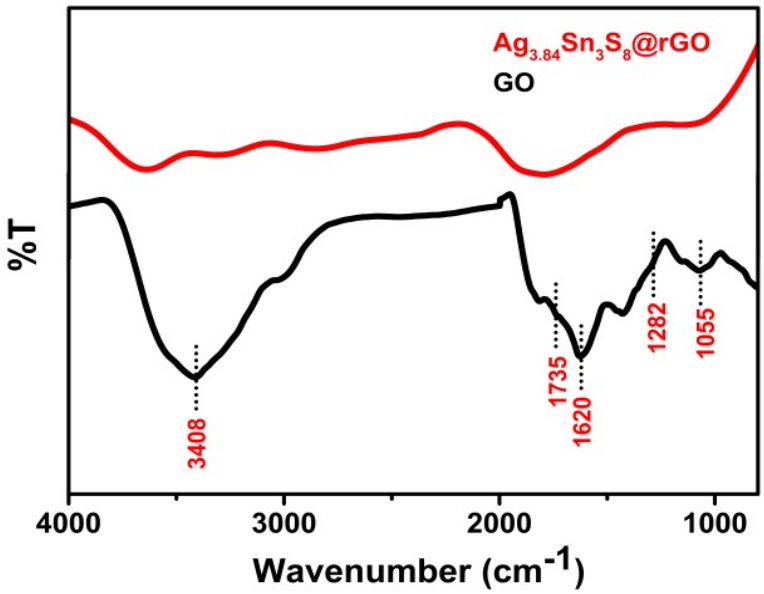

Fig. S1 FTIR spectra for GO and $Ag_{3.84}Sn_3S_8@rGO_{0.5}$ NC

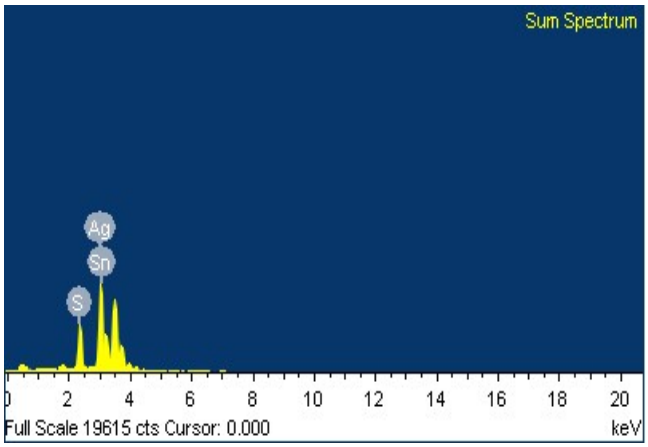

Fig. S2 EDX spectra for pure $Ag_{3.84}Sn_3S_8$

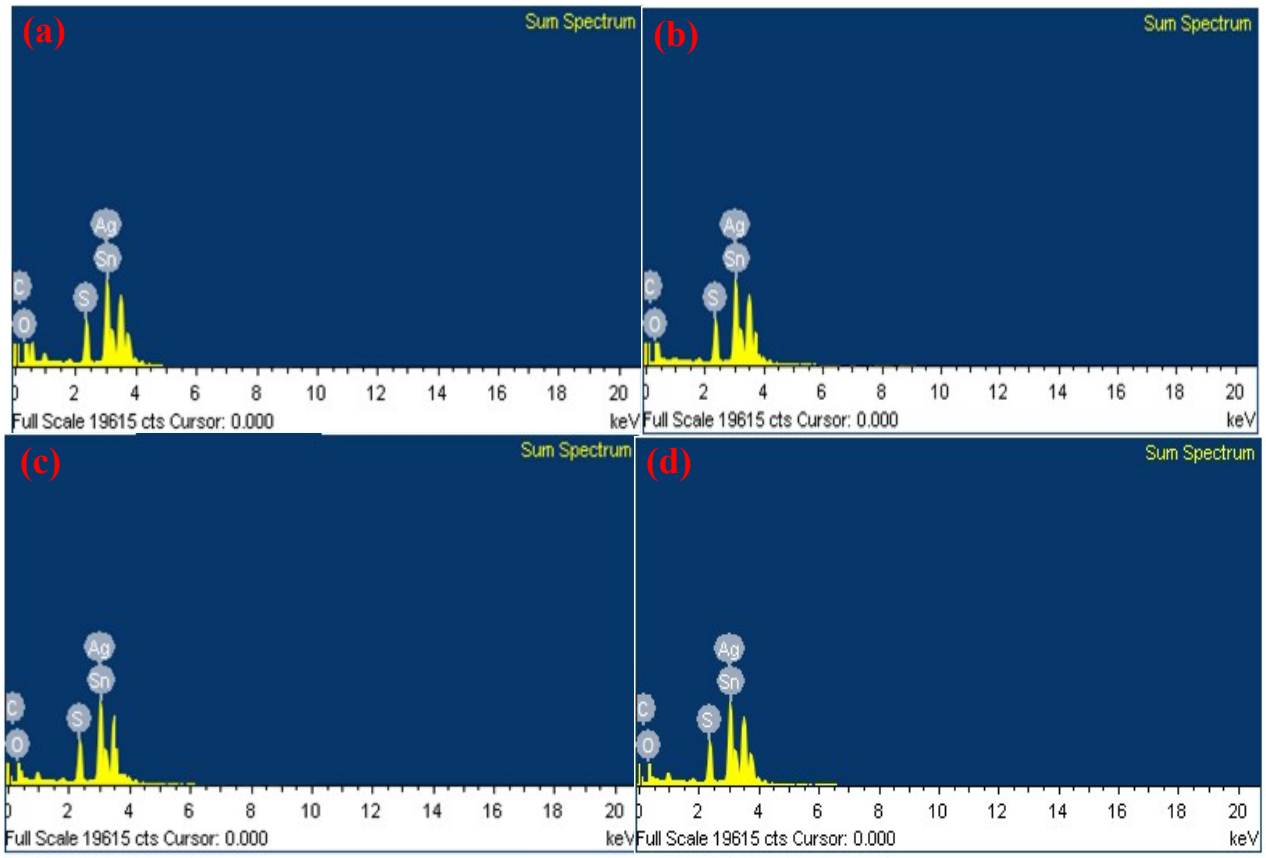

Fig. S3 EDX spectra for (a-d) $Ag_{3.84}Sn_3S_8$@$rGO_{(0.05\text{-}0.5)}$ NCs

Table S1 Elemental compositions of pure and four different $Ag_{3.84}Sn_3S_8$@rGO NCs

	Atomic %	Atomic %	Atomic %	Atomic %	Atomic %
Materials	Ag	Sn	S	C	O
$Ag_{3.84}Sn_3S_8$	22.30	20.81	56.94	0.00	0.00
$Ag_{3.84}Sn_3S_8$@$rGO_{0.05}$	22.99	21.01	55.65	0.30	0.10
$Ag_{3.84}Sn_3S_8$@$rGO_{0.1}$	21.90	20.71	56.67	0.55	0.22
$Ag_{3.84}Sn_3S_8$@$rGO_{0.25}$	22.95	21.03	54.02	1.45	0.55
$Ag_{3.84}Sn_3S_8$@$rGO_{0.5}$	20.95	18.50	57.25	2.57	0.73

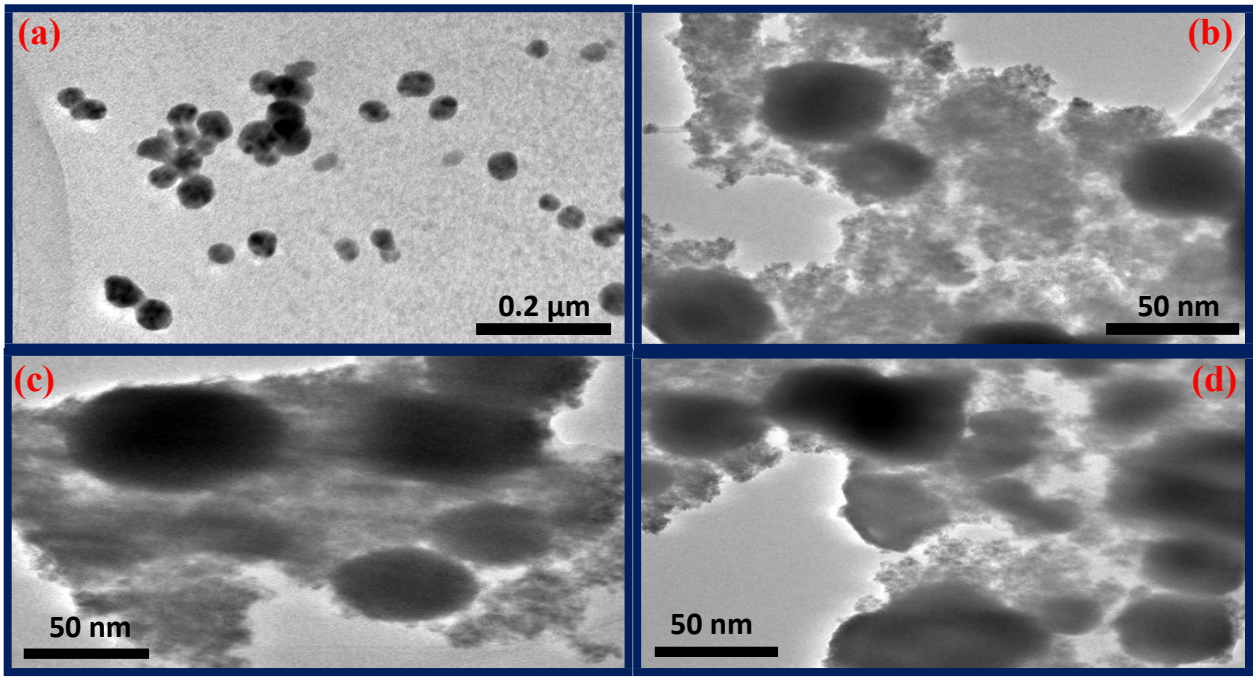

Fig. S4 (a) TEM images of (a) pure $Ag_{3.84}Sn_3S_8$ (b-d) $Ag_{3.84}Sn_3S_8$@$rGO_{0.05/0.1/0.25}$ NCs

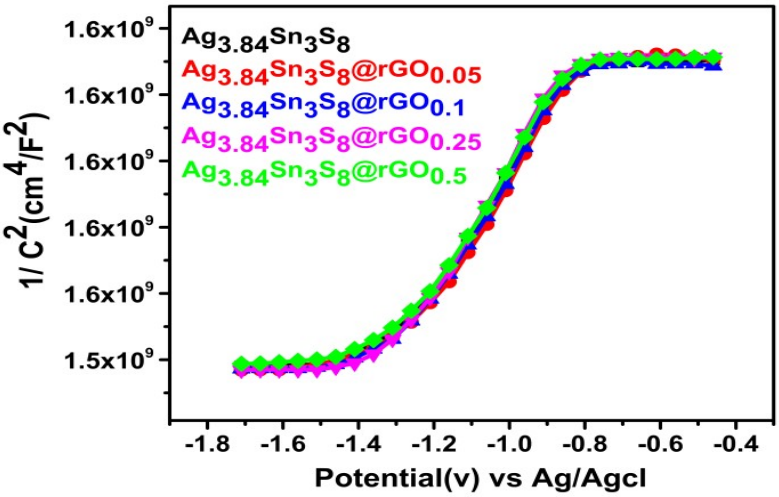

Fig. S5 Mott-Schottky plots of as synthesized materials

Table S2 The characteristic parameters obtained from Mott-Schottky plots

Materials	E_{fb} (V vs RHE)	Carrier Density (10^{10} cm^{-3})
$Ag_{3.84}Sn_3S_8$	-0.800	1.30
$Ag_{3.84}Sn_3S_8$@$rGO_{0.05}$	-0.796	1.42
$Ag_{3.84}Sn_3S_8$@$rGO_{0.1}$	-0.791	1.49
$Ag_{3.84}Sn_3S_8$@$rGO_{0.25}$	-0.785	1.67
$Ag_{3.84}Sn_3S_8$@$rGO_{0.5}$	-0.788	1.51

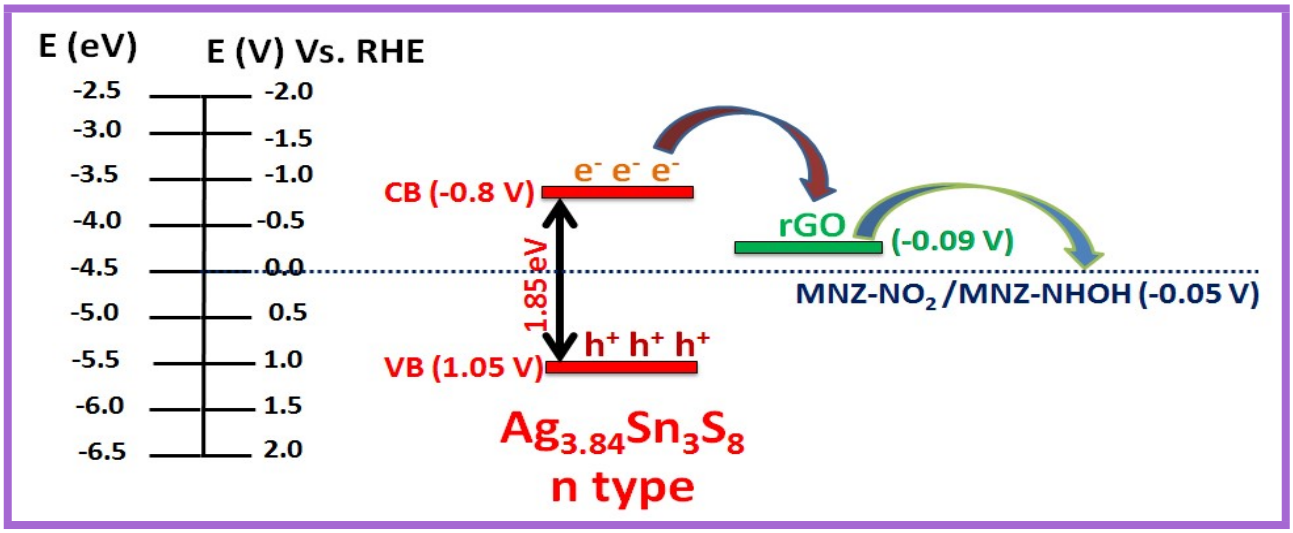

Fig. S6 Probable energy profile diagram for CB and VB levels of the catalyst and catalytic reaction pathway for detection and degradation of MNZ

With compare to pure rGO and $Ag_{3.84}Sn_3S_8$ [Fig. S8 (a) and (b)] the surface area is significantly increased in case of composites [Fig. S8 (c-f)]. Among the NCs; $Ag_{3.84}Sn_3S_8$@$rGO_{0.25}$ [Fig. S8 (e)] has the highest indicating more active reaction sites.[2] On the other hand by employing BJH analysis pore size distribution has been measured and it reveals that for pure $Ag_{3.84}Sn_3S_8$, the pore size is 21 nm but in presence of rGO the pore size becomes between 15-18 nm which further support the composite formation in hybrid material.[3]

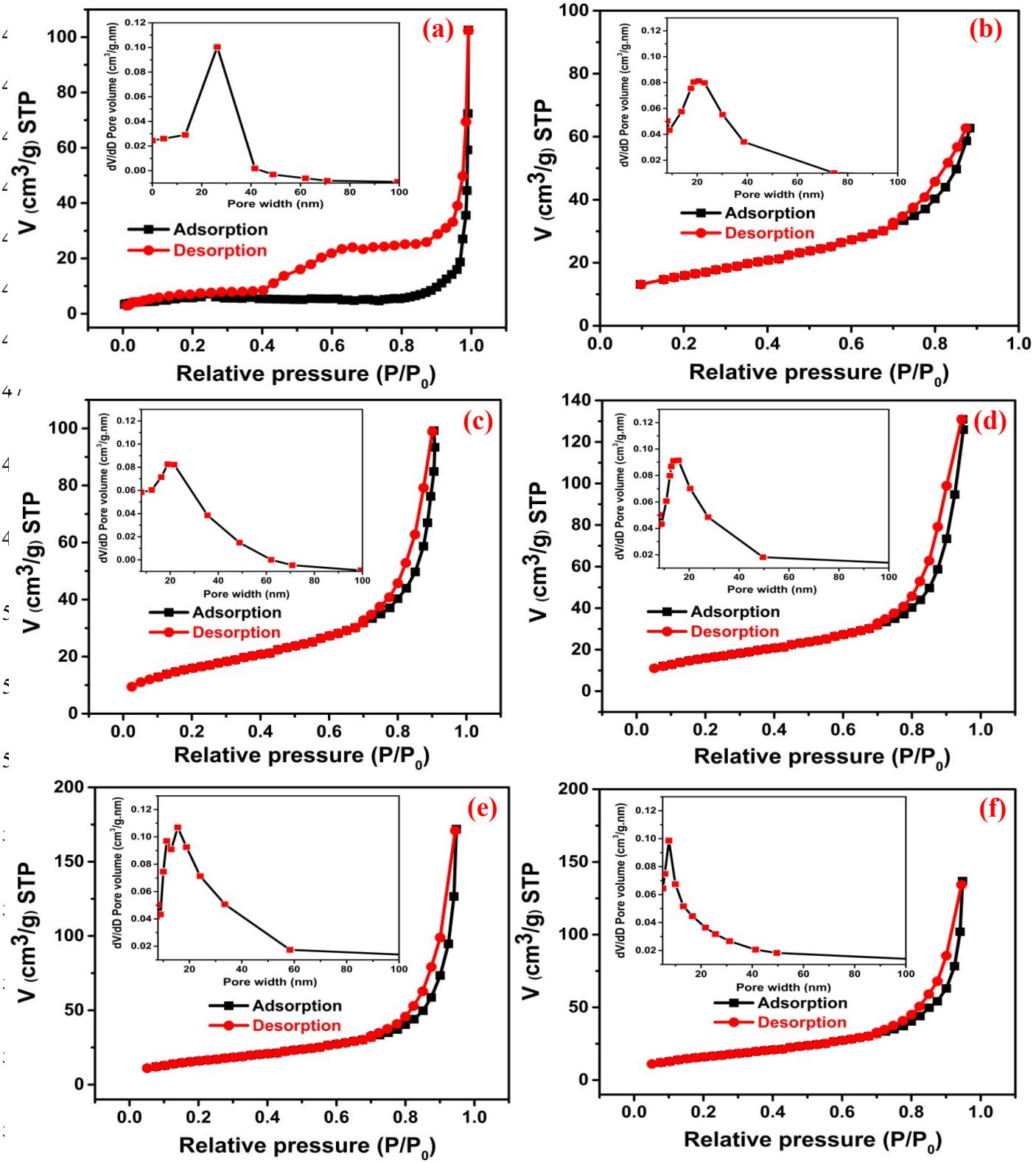

158 **Fig. S7** BET isotherms and pore size distribution analysis for (a) rGO (b) pure $Ag_{3.84}Sn_3S_8$ (c-f)

159 $Ag_{3.84}Sn_3S_8$@$rGO_{(0.05\text{-}0.5)}$ NCs

Table S3 Surface area parameters obtained from BET isotherm analysis

Materials	BET surface area (m^2/gm)	Pore size (nm)
rGO	75	25
$Ag_{3.84}Sn_3S_8$	53	21
$Ag_{3.84}Sn_3S_8$@$rGO_{0.05}$	79	19
$Ag_{3.84}Sn_3S_8$@$rGO_{0.1}$	111	18
$Ag_{3.84}Sn_3S_8$@$rGO_{0.25}$	147	16
$Ag_{3.84}Sn_3S_8$@$rGO_{0.5}$	123	15

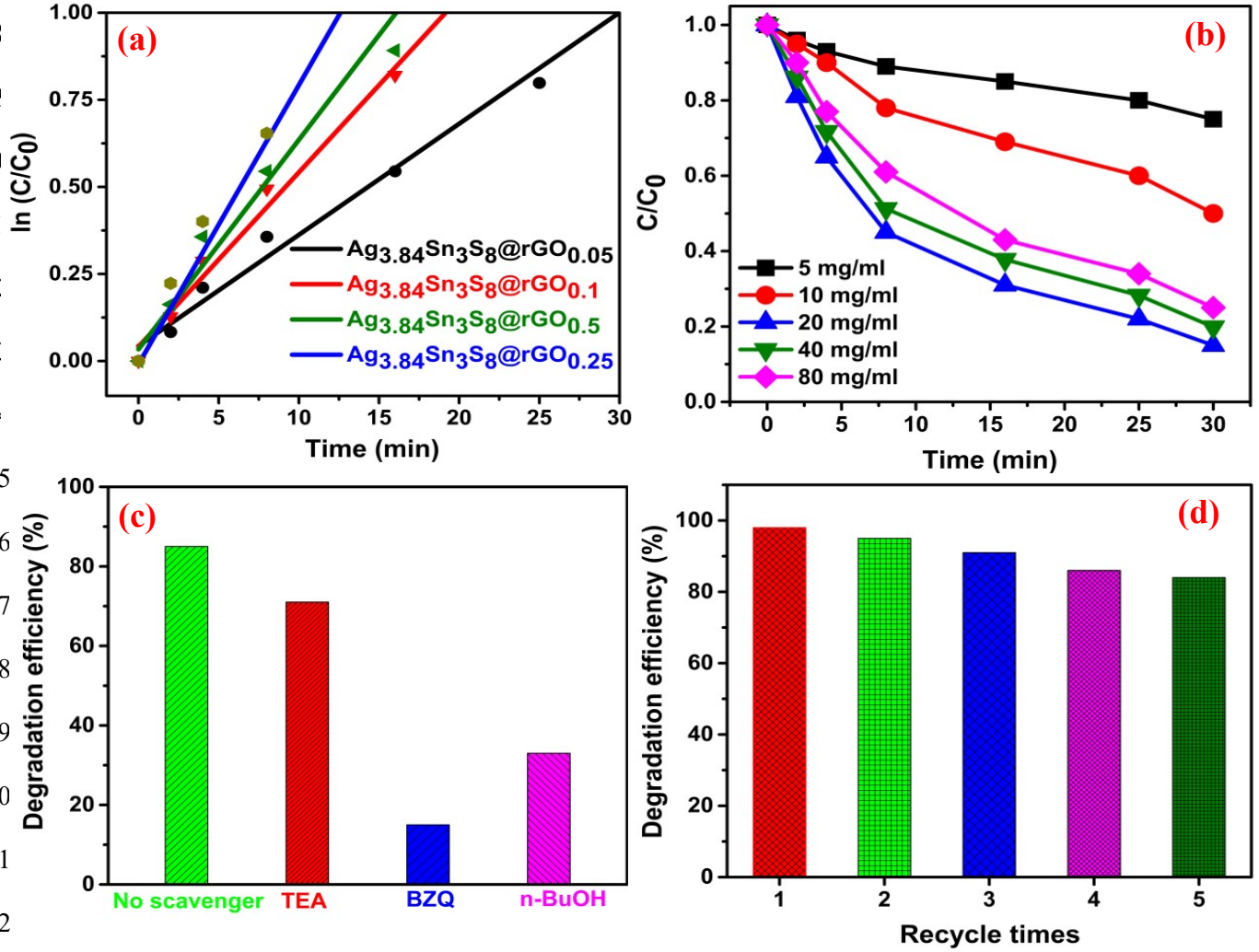

Fig. S8 (a) Kinetic study (b) effect of dosage of catalyst on photocatlytic performance (c) effect of scavengers of reactive species involved in the photodegradation (d) stability test 85

Table S4 Rate constants for the as prepared composite materials

Materials	Rate constants (k) (min^{-1})
$Ag_{3.84}Sn_3S_8$@$rGO_{0.05}$	0.0290
$Ag_{3.84}Sn_3S_8$@$rGO_{0.1}$	0.0560
$Ag_{3.84}Sn_3S_8$@$rGO_{0.25}$	0.0825
$Ag_{3.84}Sn_3S_8$@$rGO_{0.5}$	0.0625

The plausible reaction pathway for the photodegradation of MNZ

The mechanistic pathway is a crucial parameter to recognize the stepwise progress of any catalytic reaction. In accordance with the obtained results and anticipation from the previously reported studies, we have assumed the following reaction pathway for photodegradation of MNZ. At first, upon illumination of visible light the e^--h^+ pair charge separation happens [Eq. S1]. Then the e^-_{CB} and h^+_{VB} convert the O_2, H_2O to $O_2^{\cdot-}$ and ·OH respectively [Eq. S2 and S3]. Then $O_2^{\cdot-}$ reacts with H^+ to form $\cdot OH_2$ [Eq. S4]. All these radicals are ROS which degrade MNZ to its water soluble fragmentations (intermediates) and further to CO_2 and H_2O [Eq. S5-S7].

$$Ag_{3.84}Sn_3S_8@rGO + h\nu \longrightarrow Ag_{3.84}Sn_3S_8@rGO\ (e^-_{CB} + h^+_{VB}) \quad \textbf{(Eq. S1)}$$

$$Ag_{3.84}Sn_3S_8@rGO\ e^-_{CB} + O_2 \longrightarrow Ag_{3.84}Sn_3S_8@rGO + O_2^{\cdot-} \quad \textbf{(Eq. S2)}$$

$$Ag_{3.84}Sn_3S_8@rGO\ h^+_{VB} + H_2O \longrightarrow Ag_{3.84}Sn_3S_8@rGO + \cdot OH \quad \textbf{(Eq. S3)}$$

$$O_2^{\cdot-} + H^+ \longrightarrow \cdot OH_2 \quad \textbf{(Eq. S4)}$$

$$\cdot OH_2, O_2^{\cdot-}, \cdot OH, + MNZ \longrightarrow MNZ^{\cdot+} + H_2O \quad \textbf{(Eq. S5)}$$

$$\cdot OH_2, O_2^{\cdot-}, \cdot OH, + MNZ^{\cdot+} \longrightarrow \text{water soluble fragmentation of MNZ} \quad \textbf{(Eq. S6)}$$

$$\text{Water soluble fragmentation of MNZ (intermediate)} \longrightarrow CO_2 + H_2O \quad \textbf{(Eq. S7)}$$

203 **Table S5 Comparative study for photodegradation of MNZ by different photocatalysts**

204

Photocatalysts	Catalyst (g/L)	MNZ (mg/L)	Light Source (W/m^2)	Time (min)	k_{obs} (min^{-1})	Year	Ref.
TiO_2	3	80	125 (UV)	180		2015	4
TiO_2	0.5	80	125 (UV)	120	0.0233	2015	5
Fe^0/graphene-TiO_2 NW	1	35	20 (UV)	50	0.083	2018	6
TiO_2-doped Fe^{+3}	0.5	80	125 (UV)	120	0.027	2019	7
P-doped g-C_3N_4/Co_3O_4	1	10	250 (Vis)	180		2019	8
TiO_2/ZnO	1.5/0.5	10/10	100 (UV)	60	0.045/0.124	2019	9
D-g-C_3N_4-Bi_5O_7I	0.8	15	300 (Vis)	360		2019	10
$CuBi_2O_4$/CuO	1 mg/mL	50	100 mW/cm^2	120	0.0036	2020	11
Fe_3O_4/TiO_2/BC	0.35	10	16 (UV)	45	0.074	2020	12
Fe_3O_4/$rGO_{4(\%)}$/TiO_2	0.75	20	150 (Vis)	120	0.0092	2020	13
$Ag_{3.84}Sn_3S_8$@$rGO_{0.25(\%)}$	20 mg/mL	30	100 mW/cm^2	30	0.0825	2023	This work

205

206

207

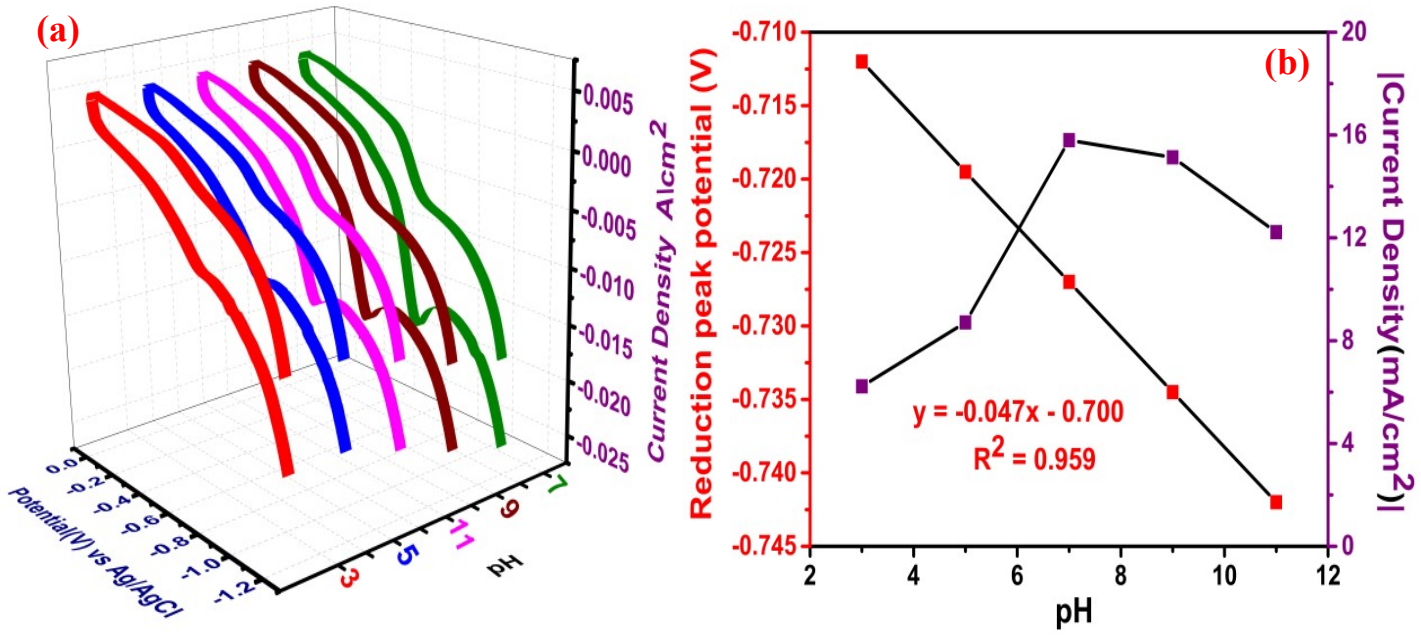

Fig. S9 (a) CV study for MNZ sensing varying pH from 3.0 to 11.0 (b) calibration plot for reduction peak potential vs pH and effect of pH on peak current density

Table S6 The MNZ recovery analysis by $Ag_{3.84}Sn_3S_8$@$rGO_{0.25(\%)}$ modified sensor (n = 3) from spiked real samples

Real Samples	Added (nM)	Detected (nM)	Recovery (%)
Lake Water	50	47.8	95.6
	100	98.4	98.4
	200	196.5	98.2
Human Urine	50	48.9	97.8
	100	99.1	99.1
	200	198.7	99.3

References

(1) B. Yang, X. Zuo, P. Chen, L. Zhou, X. Yang, H. Zhang, G. Li, M. Wu, S. Jin and X. S. Chen, *ACS Appl. Mater. Interfaces*, 2015,**7**, 137-143

(2) D. C. T. Nguyen, K. Y. Cho and W. C. Oh, *RSC Adv.*, 2017, **7**, 29284–29294.

(3) N. A. Zubir, C. Yacou, J. Motuzas, X. Zhang and J. C. Diniz Da Costa, *Sci. Rep.*, 2014, **4**, 1–8.

(4) N. Okhovat, M. Hashemi and A. A. Golpayegani, *J. Mater. Environ. Sci.*, 2015, **6**, 792–799.

(5) M. Farzadkia, E. Bazrafshan, A. Esrafili, J. K. Yang and M. Shirzad-Siboni, *J. Environ. Heal. Sci. Eng.*, 2015, **13**, 1–8.

(6) X. Wang, A. Wang, M. Lu and J. Ma, *Chem. Eng. J.*, 2018, **337**, 372–384.

(7) M. Malakootian, N. Olama, M. Malakootian and A. Nasiri, *Int. J. Environ. Sci. Technol.*, 2019, **16**, 4275–4284.

(8) Z. Zhao, J. Fan, X. Deng and J. Liu, *Chem. Eng. J.*, 2019, **360**, 1517–1529.

(9) M. L. Tran, C. C. Fu and R. S. Juang, *Environ. Sci. Pollut. Res.*, 2018, **25**, 28285–28295.

(10) M. Salimi, A. Esrafili, H. R. Sobhi, M. Behbahani, M. Gholami, M. Farzadkia, A. J. Jafari and R. R. Kalantary, *ChemistrySelect*, 2019, **4**, 10288–10295.

(11) C. Nogueira, L. E. Gomes, J. A. P. Ferencz, J. E. F. S. Rodrigues, R. V. Goncąlves and H. Wender, *J. Phys. Chem. C*, 2019, **123**, 25680–25690.

(12) F. Asgharzadeh, M. Gholami, A. J. Jafari, M. Kermani, H. Asgharnia and R. R. Kalantary, *Desalin. Water Treat.*, 2020, **175**, 304–315.

(13) F. Bashiri, M. Khejri, R. R. Kalantary and B. Kakavandi, *Journal of Molecular Liquids*., 2020, **314**, 113608.